A Breakage Model for DEM based on a Probabilistic Particle Replacement with Voronoi Fragments

Michael Denzel, Michael Prenner, Nikolaus A. Sifferlinger

Chair of Mining Engineering and Mineral Economics, University of Leoben, Austria

Corresponding author: Michael Denzel, Chair of Mining Engineering and Mineral Economics, University of Leoben, Franz-Josef-Straße 18, 8700 Leoben, michael.denzel@unileoben.ac.at

Keywords

- Particle breakage
- Comminution
- Polyhedral particles
- Discrete Element Method
- Progeny distribution

Highlights

- A replacement strategy with pre-defined breakage patterns is presented.
- Progeny distribution can be predicted with high accuracy.
- Mass and volume remain constant and multiple breakage can be simulated.
- Polyhedral particles of any shape can be used.
- The model was validated with various trials with different batches of sinter.

Abstract

Due to mechanical stress, bulk material is crushed and fines are produced. This can either be desired in comminution processes or undesired in conveying and storage processes. In this work a novel breakage model for the Discrete Element Method is presented to allow a prediction of the resulting particle size distribution after damaging events. The breakage model is based on a probabilistic particle replacement strategy. Depending on the load, the initial particle is replaced by a breakage pattern tessellated with the Voronoi algorithm. Replacement probabilities and breakage patterns follow results from breakage tests. In contrast to other replacement models, mass and volume remain constant. Initial particles are polyhedral and can be of any shape. Crushing processes with multiple breakage can be simulated. The computational scheme is described in detail. The model was verified and validated with trials of shatter tests and two conveying processes with blast furnace sinter from two different industrial partners.

1. Introduction

The Discrete Element Method (DEM), originally proposed by Cundall and Strack [1], is a powerful tool for investigating phenomena occurring at the scale of particle diameter and simulating bulk behavior. Thus, DEM has become widely established as an efficient method addressing a variety of engineering problems with granular and discontinuous materials like granular flows, powder mechanics or comminution [2–4].

In many processes mechanical degradation or breakage occurs, so the phenomena cannot be described by DEM alone. When particle breakage does not affect flow or bulk material behavior, DEM and breakage can be decoupled, so that breakage can be investigated in a post-processing procedure. An approach where the compressive force is evaluated after simulation is described in [5, 6]. Another example of decoupling DEM and breakage is a population balance model used for different types of mills in [7–10].

In some cases, particle breakage affects flow or bulk behavior of the material, so that an embedded description of breakage in DEM is necessary. This is the case in various systems, especially in comminution processes [11–14] and transport or storage processes of blast furnace sinter [15–17], for example. Material degradation and fines generation could lead to air pollution, risk of dust explosions, high costs and emissions. This is particularly the case for blast furnace sinter handling because fines have to be re-sintered again, which is a highly energy demanding process. Minimizing material degradation during conveying processes would lead to a major cost reduction and massive savings in energy and CO_2 emissions [17–19].

Different approaches have been developed to describe breakage embedded in DEM. These can be grouped into those in which the progeny fragments are resolved throughout the DEM simulation and those in which fragments only appear when a critical condition is met [20]. The most established model for the former group is the Bonded Particle Model (BPM) [21], which is well suitable to mimic the behavior of agglomerates containing of cemented granular materials [22–28] and has also been used for mills [29, 30] and crushers [31] or even dynamic belt simulations [32]. Further examples for the former group are the Bonded Cell Method [33] and the Discrete Grain Breakage Model [34].

The second group is represented by particle or fragment replacement methods [35]. In the Particle Replacement Model (PRM), originally proposed in [36, 37], the particles are “instantaneously” (within the duration of one time step) replaced by several smaller progeny particles when the criterion for failure is met. The progeny particles can be spheres or clumped spheres [11, 12, 35, 37–40], superquadrics [41] or polyhedral cells [42–45]. The failure criterion could be the excess of a critical force, for example. A major benefit of the replacement method is that the progeny sizes can be defined, so any fragment size distribution can be achieved. Another advantage is that no additional calibration is needed like for other breakage models, such as the BPM.

The particle replacement approach was used to describe particle breakage under confined conditions [38, 46, 47], geotechnical applications [48] and comminution equipment including different types of crushers [12, 13, 41, 49]. The vast majority of PRM uses spheres as progeny particles for computational efficiency. The major disadvantage hereby is, however, the volume loss when a large sphere is replaced by several smaller spheres. To ensure mass constancy, the fragment density was adjusted in [50], which is negligible in mills and crushers, but less suitable for conveying processes because flow behavior and loads on conveying equipment would be distorted. In the work of Tavares et al. [20] volume and mass constancy is ensured by overlapping the following smaller

spheres and defining damping factors for the following time steps to avoid explosions. Further limitations of spherical particles are the description of particle shape and applications when multiple breakage or further breakage of fragments occurs, which is not the case for polyhedral particles [51]. On the other hand, the replacement by spheres is advantageous in terms of computational efficiency. With spherical particles the smallest effort in contact detection and force calculation is necessary and a straight forward conversion to size distribution is possible [51].

Based on the Tavares Breakage Model [52], a model was implemented in DEM in [53, 54] where the Voronoi subdivision algorithm [55–58] is used for mass and volume conservation, which was validated in [59] for single particle drop weight tests. In [45] breakage tests were simulated using polyhedral particles and Voronoi tessellation. Potapov and Campbell introduced a model involving polyhedral particles in [44, 60] called the Fast Breakage Model (FBM). It was used to describe breakage in particle beds in [61, 62] and to simulate comminution equipment in [43, 63]. A comparison of the BPM, PRM and FBM is provided in [64]. In the Discrete Breakage Model (DBM), which is based on [60, 65], the particles are discretized into a number of elements of simple geometrical shapes. The DBM was validated in [66].

In this work a breakage model is presented, which uses polyhedral particles and probabilistically replaces these with Voronoi tessellated breakage patterns if a critical condition is met. The model was first presented in [67–69] and is described in detail in [70] which is a PhD thesis in the evaluation process at the time of writing. The model allows to simulate particle breakage embedded in DEM. Various processes like conveying or comminution processes can be simulated efficiently in order to predict the resulting particle size distribution (PSD) with high accuracy.

2. Single particle impact tests

For detailed investigations of particle breakage behavior, single particle breakage tests are recommended [71], especially for the prediction of comminution machine performance [72]. Depending on the case of loading, a suitable test method has to be performed. For impact crushers and transportation and handling processes [73], single contact impact tests like drop tests [16], pneumatic guns [74] or tests with rotary impact testers [75, 76] are performed. For most other comminution processes, double contact tests like drop weight, impact load cell [52] or slow compression tests are performed.

The model was originally developed to simulate the degradation of sinter in order to predict the resulting fragment size distribution and fines generation due to transport and storage processes. Thus, single contact impact tests were conducted for this application with a specially developed automated single particle impact tester [77]. The test rig consists of a vibratory bowl feeder to separate the bulk sample, weighing station, air cannon, drop module and integrated fragment analysis by a specially developed vibrating sorter. The high grade of automation allows rapid single particle breakage characterization. A detailed description of the test rig and breakage test results for blast furnace sinter including breakage probability, fragment size distribution, fines production, size-independent relative fines production and characterization with the t_n-model [78] is provided in [70, 77].

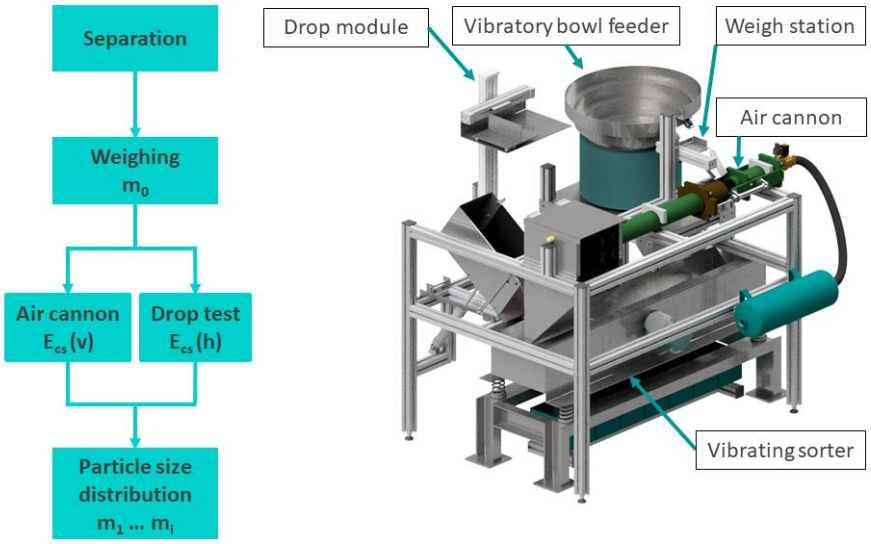

Figure 1: Concept of a highly automated single particle impact tester [77]

3. Probabilistic particle replacement with breakage patterns

In order to simulate breakage embedded in DEM with high accuracy in terms of fragment size distribution, in high mass flows and a reasonable computing efficiency, a novel particle breakage model has been developed. The model is based on a probabilistic particle replacement with fragments, which are previously tessellated with the Voronoi algorithm. The model has been developed using the DEM software ThreeParticle with a particle replacement API (Application Programming Interface) in C++. The model uses the recently implemented Voronoi tessellation tool in ThreeParticle. The model was first presented in [67–69] and is described in detail in [70].

3.1. Concept

For Voronoi tessellation, polyhedral particles are required. In this case the initial particles are of spherical shape (resolution of 18 for both rotational axis), but can be of any convex shape. Depending on the stress, initial particles are probabilistically replaced by different particles, similar to [20, 40]. In contrast to [20, 40] and other particle replacement models, the initial particle is replaced by different breakage patterns instead of several smaller spheres. The different breakage patterns have the same mass and volume as the initial particle, which ensures mass and volume constancy. The breakage patterns are predefined and are copies of the initial particle, but have been tessellated with the Voronoi algorithm (see Figure 2). The replacement with previously defined breakage patterns is much more efficient in terms of computational effort than tessellating the particle at the event of breakage, which would mean that the Voronoi algorithm would have to be performed at every event of breakage.

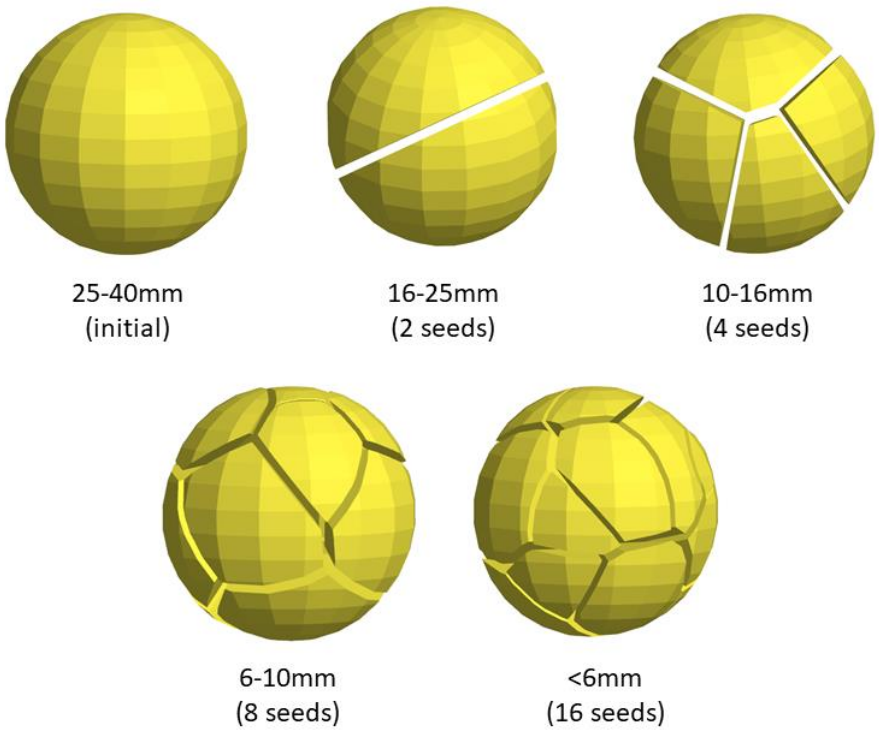

Figure 2: Breakage patterns, which are Voronoi-tessellated polyhedral particles [69]

The Voronoi algorithm is an efficient way to tessellate areas or volumes. For Voronoi-tessellation, randomly distributed points (seeds) are generated. Then the area or volume is divided in the middle of two neighboring seeds. Thus, the average fragment size in this application depends on the number of seeds. The fragments are sharp-edged polyhedral particles and are of random shape. This requires more computing power and usually smaller simulation time steps than with spheres, but ensures mass and volume constancy. No fictive overlaps and temporary damping factors are necessary for the fragments to ensure volume constancy, as needed for a replacement with spheres.

In the here presented example which is shown in Figure 2, size fractions defined by their passing diameter of a conventional screen are defined. It must be stated that due to the random shape of individual fragments, individual fragment masses do not correspond to average particle mass in the respective size fraction. To ensure that the average fragment mass within a breakage pattern approximately corresponds to the average particle mass in the respective size fraction $m_{fraction}$, the number of seeds s can be defined by Equation (1), with m_0 as the initial particle mass.

$$\lfloor s \rceil = \frac{m_{fraction}}{m_0} \tag{1}$$

In Figure 2 a particle of 40 mm corresponding to the initial particle size fraction 25-40 mm is depicted. Four different breakage patterns were defined for the different resulting fragment sizes corresponding to the size fractions 16-25, 10-16, 6-10 and <6 mm. To

reduce computing power, fines are represented larger and summarized as 6 mm fragments in this case.

Depending on the stress, the initial particle is completely replaced by fragments of a defined size. The probability for each breakage pattern or resulting fragment size is determined from breakage test results, which were obtained from single particle impact tests with the test rig described in Section 2. A piecewise linear regression is conducted in order to allow simple calculation of the replacement probability at any specific impact energy Ecs using linear interpolation (see Figure 3).

The piecewise linear regression was conducted with Matlab by means of [79] using the least squares method, in which the breakpoints have to be defined by the user (in this case at Ecs = 14 J/kg and Ecs = 49 J/kg). The linear equations resulting from this Matlab calculation were then slightly adjusted manually in order to ensure that the sum of all probabilities is 100 at every point. This was achieved by adjusting the gradients that the sum of all gradients in all intervals was 0. These linear equations were then implemented in the particle replacement API. The adjustment is simple and can be performed manually for linear regressions, but could be mathematically complex for other types of regression, which could be more accurate in some cases. For this application a linear regression was considered sufficiently accurate.

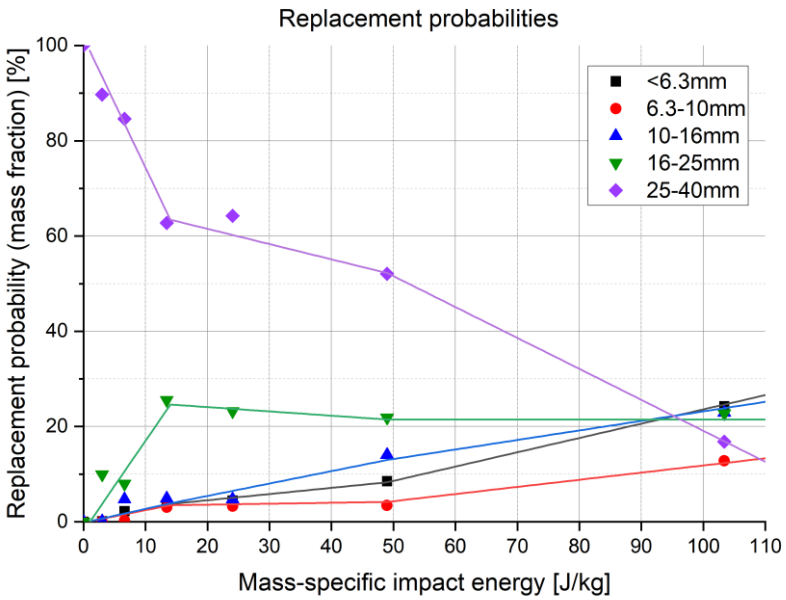

Figure 3: Replacement probabilities for following particles from piecewise linear regression based on breakage test results in [69, 70]

At every compressive force maximum, a corresponding impact velocity and a specific energy is calculated. If the maximum compressive force exceeds a minimum breakage force, a random algorithm is started. At the event of breakage, one of the predefined breakage patterns is determined by the random generator. The probability for each breakage pattern is equivalent to the average mass fraction of the corresponding fragment size after impact at this specific impact energy. When the initial particle size is determined

by the random generator, no replacement occurs. This leads to the correct PSD in the bulk sample, when applied on a high number of particles.

In Figure 4 the breakage model is demonstrated with the impact of sinter particles on a steel plate. As the model is based on probabilities, a number of particles are necessary. The impact of 25 identical initial particles (40 mm in diameter, 47 g) is simulated at different velocities. Figure 4 shows the particles before the impact, moving towards the steel plate. Figure 4b)-d) show the particles after the impact with different velocities, moving away from the steel plate. The color scale represents the particle or fragment mass (0 to 47 g). Shortly after the impact process is completed, the initial particles are replaced by one of the breakage patterns from Figure 2, following the probabilities of Figure 3. The initial 40 mm particles appear red, the 16-25 mm fragments appear green and all smaller fragments (10-16, 6-10, <6 mm) appear blue in this case.

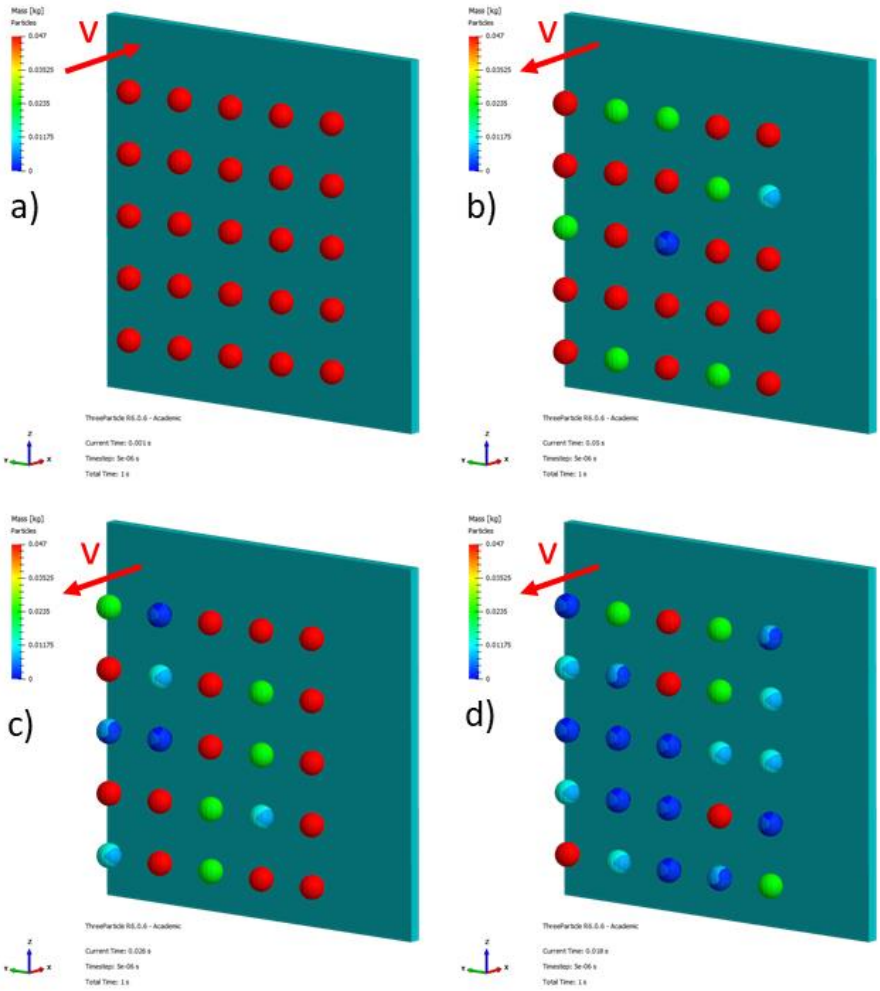

Figure 4: Impact simulation with 25 identical initial particles with d=40 mm and m=47 g a) before impact and after impact with b) 5 m/s (12.5 J/kg) c) 10 m/s (50 J/kg) d) 15 m/s (112.5 J/kg). Color scale represents fragment mass from 0 to 47 g [70]

3.2. Correlation between impact velocity and compressive force

The relation between maximum fictive compressive force at an impact and impact velocity is determined by impact simulations with different velocities. In contrast to smooth spheres, the compressive force depends on the alignment for polyhedral particles. For this purpose, the impact simulations were conducted with 1000 particles with random alignment. Then the median value of the maximum compressive forces is used.
Depending on the contact model, different correlations are determined. For polyhedral particles, the Hooke contact model is strongly recommended [70]. If the Hooke model is used, the maximum compressive force *maxCF* is linearly dependent on the impact velocity *v* following Equation (2). The linear parameter *a* was determined for different particles, which differ in shape and mass. If the linear parameter *a* is plotted against the particle mass *m*, a power trend is noticed (see Figure 5). Another linear parameter *A* and the exponent in this power trend depend on simulation parameters. The linear parameter *a* is normalized in Figure 5. The linear parameter *a* is only dependent on the particle mass *m* and is independent of the particle shape. This fact significantly reduces pre-simulation effort to determine the correlation between maximum compressive force *maxCF* and impact velocity *v*, especially for simulations when the fragments are further breakable (multiple breakage).

$$maxCF = a\,v \tag{2}$$

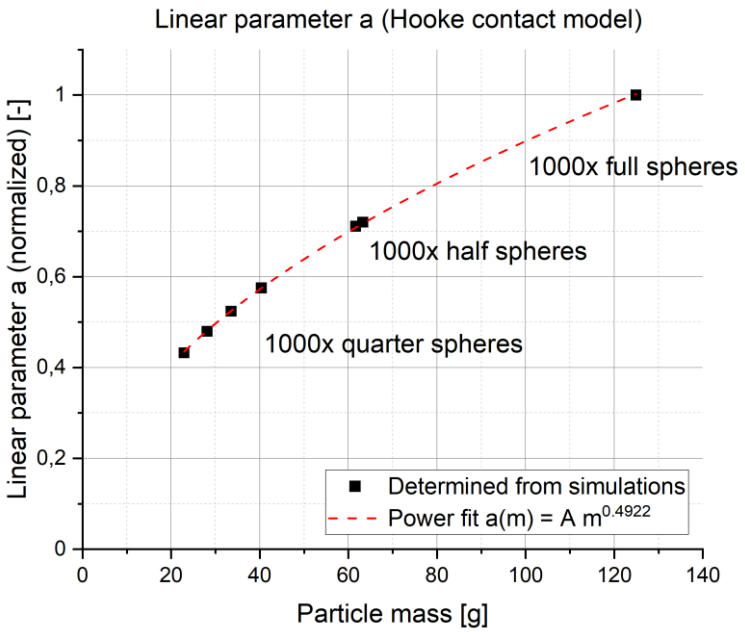

Figure 5: Mass dependency of the linear parameter *a* for the correlation between maximum compressive force *maxCF* and impact velocity *v* with the Hooke contact model following Equation (2.

A detailed comparison of the Hooke and Hertz-Mindlin contact model for impact processes is provided in [70]. The Hertz-Mindlin model could lead to extraordinarily high contact forces in some cases for sharp-edged particles, especially from a certain impact velocity. The Hertz-Mindlin model is suitable for particles with smooth surfaces, which is consistent with statements in [80]. The Hooke model leads to higher and more widely dispersed contact forces than the Hertz-Mindlin model, but does not lead to extraordinary contact forces due to sharp edges. Thus, the Hooke model is more suitable for particles with non-smooth surfaces.

3.3. Energy balance

In contrast to reality, the fragments in Figure 4 do not fly apart in this case. This is due to the fact that the replacement occurs a few time steps after the impact process is completed, which is necessary to avoid unrealistic explosions and a false increase in kinetic energy. If the particle were replaced by smaller fragments during the impact process, which would mean that there was still a certain overlap with the impact surface, this could lead to extraordinarily high overlaps for the small fragments with the impact surface and thus to extraordinarily high reaction forces and explosions.

If the replacement occurs after completion of the impact process, the kinetic energy of the fragments after the breakage is also higher than in reality. The fragments all have a similar velocity after impact, which is only reduced by a damping factor calculated from the coefficient of restitution. Thus, it must be stated that the energy balance is not correct unless the breakage energy is taken into account because the proportion of kinetic energy is too high then.

One method to consider the breakage energy would be to decrease the velocity after the impact by a factor, which could easily be implemented with the API. Therefore, further investigations regarding the breakage energy would be needed. Alternatively, the breakage energy could be estimated by means of the Griffith criterion [81], whereby the breakage energy is proportional to the creation of new surfaces [82] with a given surface energy.

Breakage with fragments flying apart could be visualized with this model by defining an initial overlap among the Voronoi fragments. This could be defined by an offset, which shifts the Voronoi fragments toward or away the center of the particle after tessellation. Figure 2 was created with an explosion offset of +2 mm for better visualization, for example. A negative explosion offset would lead to overlaps among the Voronoi fragments.

3.4. Fragment size analysis

Due to the Voronoi tessellation process, fragments are of random shape and individual fragment sizes vary. In contrast to other breakage models where spheres are used and fragment sizes can be simply determined by diameter, mass or volume, in this model fragment sizes can only be identified by particle names. When particles are defined, every particle is assigned a name containing its size in the first characters, for example. Thus, also for breakage patterns a name corresponding to their size fraction must be assigned. In ThreeParticle the Voronoi fragments resulting from a tessellation are numbered and the name of the initial particle with the suffix _voronoi_x is automatically assigned. Here x is the number of the fragment, which starts the count at 0. Thus, every fragment can later

be associated with its breakage pattern and categorized into a certain size fraction, independent of its actual size and mass in the simulation. Fragment size analysis can then simply be conducted during post-processing. For this purpose, only the particle masses and names have to be analyzed. Most DEM programs provide tools for this purpose like PSD sensors, for example.

4. Multiple breakage

For longer and complex conveying processes with several damaging events, it can be necessary to generate further breakable fragments. The model presented here allows further breakage of fragments as the generated fragments are also polyhedral particles, which are able to be further tessellated with the Voronoi algorithm.

As individual fragments have different masses and shapes, for each fragment a correlation between impact velocity and compressive force has then to be determined, following the procedure described in Section 3.2 using the Hooke contact model. Evaluations revealed that also for very irregularly shaped and sharp-edged fragments impact simulations with 1000 fragments with random alignment were accurate enough. Maximum compressive force values are more widely dispersed in this case, which reaffirms using the mean value instead of the average value to reduce the impact of outliers.

How often a particle and its resulting fragments can be further broken is described with the breakage level L in the following. For example, a breakage level of L=2 means that the initial particle for this breakage process is a fragment of a previous breakage process at L=1.

In Figure 6 multiple breakage for a 50 mm particle of spherical shape is exemplarily shown. At breakage level L = 1 the initial particle is able to break into one of five breakage patterns (40, 25, 16, 10, 6 mm), which are aligned below the initial particle in Figure 6. Breakage by replacement of a breakage pattern tessellated from the same particle is indicated with a black line (Voronoi tessellation). When the 50 mm initial particle breaks into the 40 mm size fraction, two seeds are generated (s = 2), which results in two fragments approximately shaped like a half sphere, in this case. The particles in the 40 mm size fraction are then further breakable into the four smaller size fractions at breakage level L = 2. When the 40 mm size fraction breaks into the 25 mm size fraction, again s = 2 is applied, which splits the half spheres into quarter spheres in this case. The 25 mm size fraction is then further breakable into the three smaller size fractions at breakage level L = 3. When the 50 mm particle directly breaks into the 25 mm size fraction, it is replaced by a compound particle assembled from its further broken fragments to ensure that the same fragments are generated as from breakage in two steps (via L = 1 and L = 2). L = 4 would be further breakage of the 16 mm size fraction in this case, which was not implemented here. As fragment size distribution is determined by names of particles during post-processing (with Matlab routines, for example), the assignment of suitable particle names is very important for this model.

The number of required correlations between impact velocity and maximum compressive force *c* also depends on the number of seeds *s*, which describes how many fragments are generated at a breakage process. The number of correlations *c* can easily exceed to high numbers requiring high calibration and pre-simulation effort. For a

constant number of seeds *s* for each breakage level *L*, the number of required correlations *c* follows Equation (3). However, considering the fact that the linear parameter in Equation (2) is only dependent on the particle mass and independent of the particle shape (see Section 3.2), only a few impact simulations have to be conducted until a trend for the linear parameter *a* can be fitted. Then the linear parameter a can then be easily calculated for each particle with the particle mass *m*. Once the linear parameter *a* is calculated, the correlation between maximum compressive force *maxCF* and impact velocity *v* can be calculated with Equation (2).

$$c(s,L) = \begin{cases} 1, & L = 1 \\ \sum_{i=1}^{L-1} s^i + 1, & L > 1 \end{cases} \quad with\ s, L \in \mathbb{N} \tag{3}$$

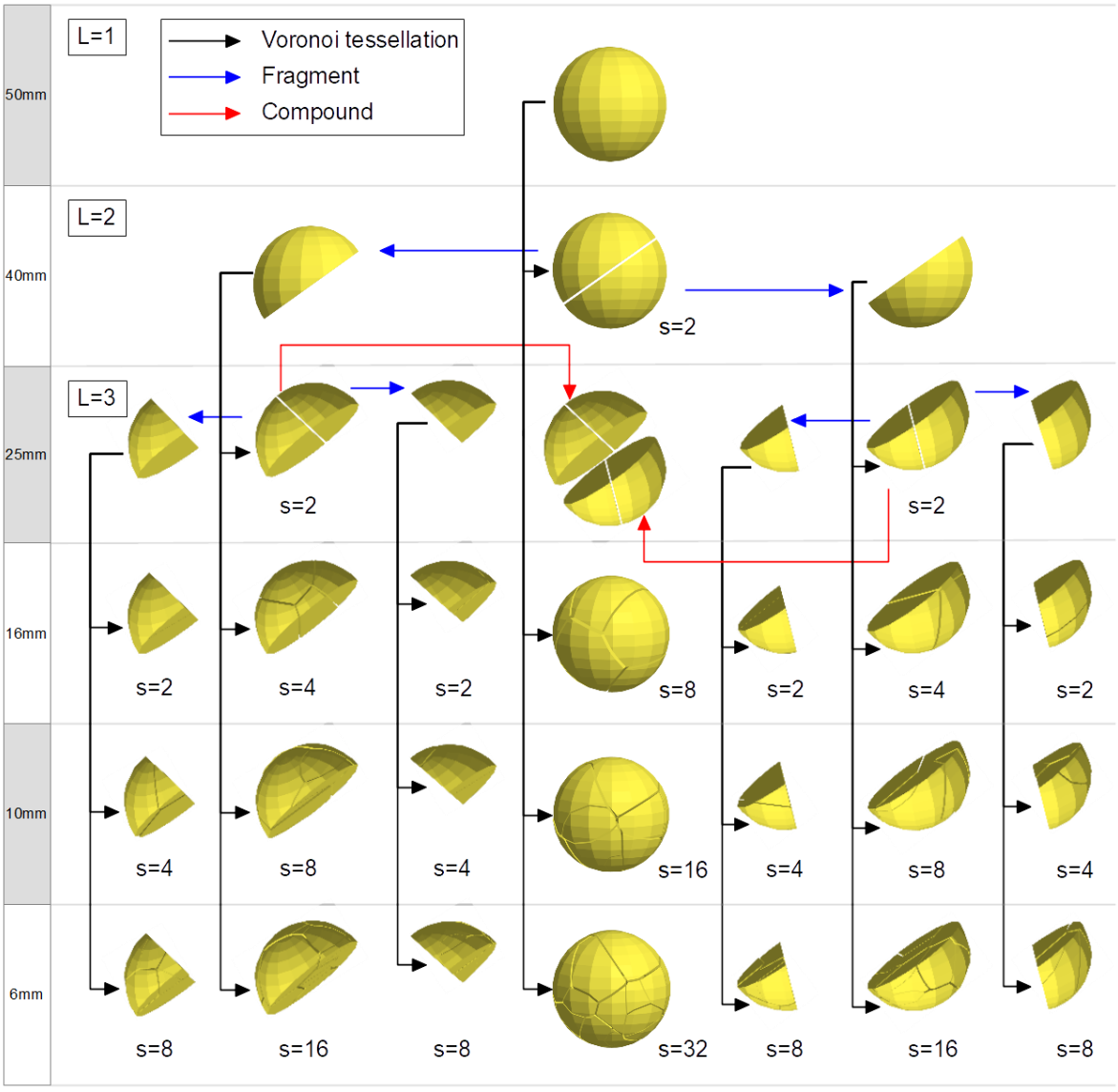

Figure 6: Multiple breakage on 3 breakage levels (L=3) [70]

5. Computational scheme

The breakage model was developed using ThreeParticle's particle replacement API, which allows the user to extend the simulation software with additional features. Customized functions can be programmed with C++ in the API and will be inserted into the default calculation cycle of the DEM software ThreeParticle.

5.1. Custom properties

In ThreeParticle custom properties have been introduced to ease the user's handling of custom variables, which are stored as a common string and can be easily written and read via predefined functions [83]. The custom properties are not deleted when a new simulation cycle starts. In this case, the custom properties are used to take into account the particle history. The custom properties string is assembled from comma-separated values and is converted into a vector of type double with four entries. A description of the custom properties vector is given in Equation (4). In various steps values (type double) are written to and read from the custom properties vector. The first two entries customProperties(0,1) are updated at the end of the algorithm. This is done by replacing the first value customProperties(0) by the second customProperties(1) and by writing the current compressive force into customProperties(1). *CF(t-2)* describes the compressive force two time steps before. *CF(t-1)* is the compressive force one time step before.

$$customProperties = \begin{pmatrix} CF(t-2) \\ CF(t-2) \\ maxCF \\ Breakage\ timer \end{pmatrix} \tag{4}$$

5.2. Breakage delay

The breakage delay is necessary to avoid extraordinarily high overlaps and explosions due to almost instant replacement (delayed by one time step) as described in Section 3.3. To implement a breakage delay in the algorithm, a breakage timer is introduced, which is reduced by 1 each time step. The value for the breakage timer or breakage delay is dependent on maximum velocities, particle size and time step. A breakage delay of 50-100 was defined for the simulations presented in this work.

5.3. Breakage algorithm

A schematic flow diagram of the algorithm of the model is depicted in Figure 7. All computational procedures before or after this Plugin are summarized as previous or following computation steps of the DEM software in this flow diagram. The computational scheme is executed in every simulation cycle and parallelized for every single particle.

In the first step it is checked if the particle is defined as breakable, by comparison of the particle name with predefined Strings, which correspond to the names of the breakable particles. If not, the whole particle replacement procedure including several if-clauses is skipped for this certain particle, which reduces computational effort.

If the particle is defined as breakable, its custom properties are checked. Generally, when a new particle is created, no custom properties are assigned by default. Thus, the custom properties are empty (no value) for new particles, which leads to errors when

compared with values of the type double. Therefore, the custom properties have to be initialized with 0 values for newly created particles. In the next step the current compressive force *CF* on the particle in this time step is compared with a minimum value for breakage. The minimum compressive forces for breakage are calculated with the linear parameter a from Equation (2) and from minimum mass-specific impact energies for breakage, which are determined from drop tests in [77].

Then it is evaluated if the compressive force *CF* peaked in the previous time step (t-1). For this purpose, the compressive force values of the two time steps before (t-2) and (t-1) from customProperties(0,1) are compared with the current compressive force in this time step *CF(t)* with the condition in Equation (5).

$$CF(t-2) < CF(t) < CF(t-1) \tag{5}$$

If a peak for the previous time step (t-1) is detected, the maximum compressive force value *maxCF* in customProperties(2) is set as CF(t-1) and the breakage timer is set to a defined value (see Section 5.2).

When the breakage timer is 1 and a value is set for the maximum compressive force (maxCF≠0), the actual particle replacement procedure starts. With the correlation from Equation (2), the impact velocity *v* is back-calculated. Then the mass-specific impact energy *Ecs* is calculated with the impact velocity *v* and Equation (6). With a given specific impact energy *Ecs* the breakage probabilities for each breakage pattern can be interpolated (see Figure 3).

$$E_{CS} = \frac{v^2}{2} \tag{6}$$

Then a random procedure is started. It has to be considered that there is no real randomness in numerics and random generators are actually pseudo-random generators, which deliver the same set of values depending on the seed. Always different sets of values can be obtained when the pseudo-random generator is seeded with a value depending on the absolute time, for example. Most pseudo-random generators deliver normally-distributed values, which is not desired here. Evenly distributed values are needed. For this model the Mersenne Twister MT19937 is used [84], which is an equidistributed uniform pseudo-random generator. A pseudo-random value is generated in the range of 0 to 10000.

With the previously calculated replacement probabilities, intervals in the range of 1 to 10000 are then defined for comparison with the pseudo-random value. Each interval corresponds to a different breakage pattern. Depending on the pseudo-random value, a breakage pattern is selected and the initial particle is replaced. For the following particle, all custom properties are set 0.

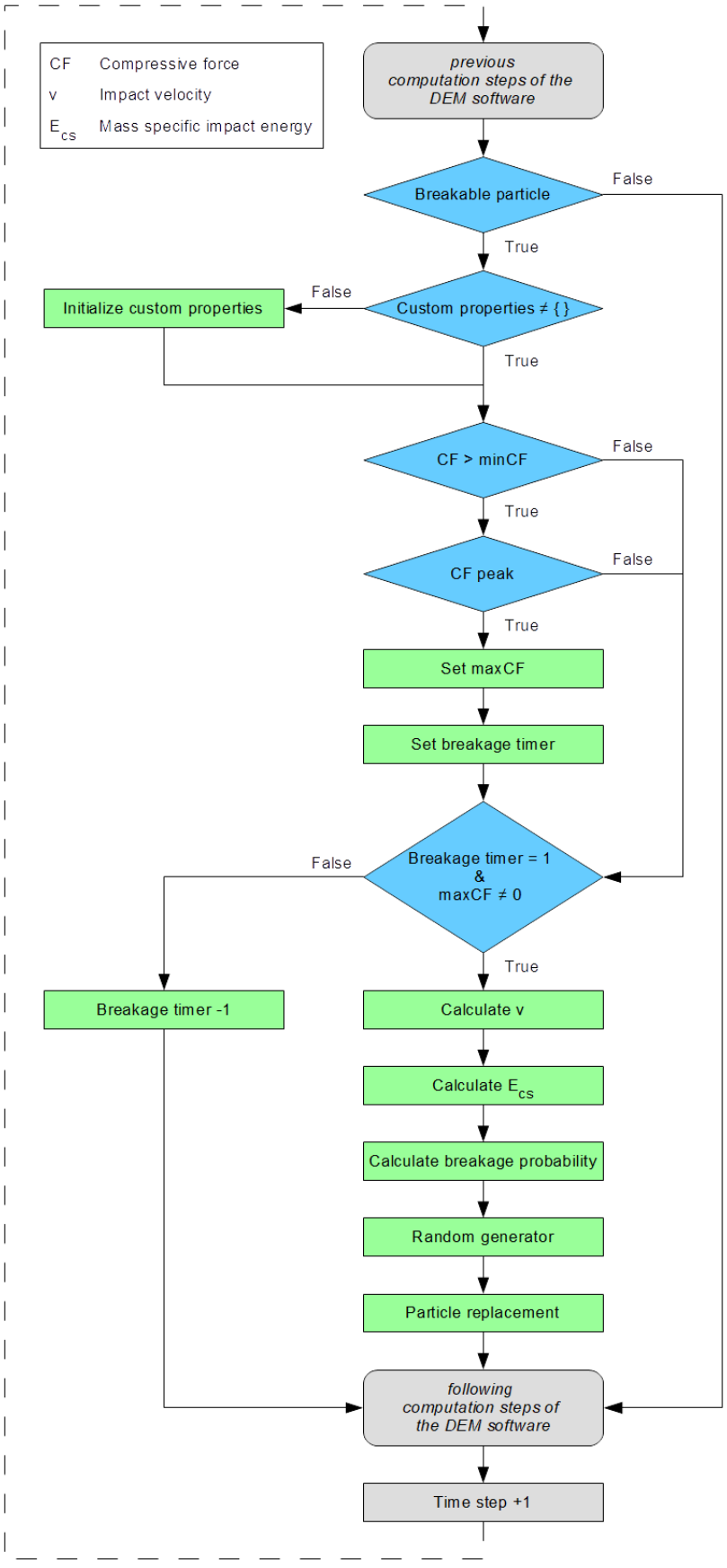

Figure 7: Schematic flow diagram of the breakage algorithm [70]

6. Verification and Validation

The novel breakage model was verified and validated with a trial of shatter tests. Furthermore, simulations of conveying trials which are described in [5, 6] including a standard chute and a dynamic transfer system (FlowScrape) were repeated with the novel breakage model and compared with results from the experiments for further validation. The content of this Section was first published in [67–69].

In the shatter tests, a drop apparatus with a quick-opening flap from [85] was used (see Figure 8). The drop apparatus had a drop height of 3.8 m and the bulk material was dropped onto a steel plate at the bottom. The flap was held closed by an electromagnet and was quickly opened by gravity, when triggered. Three tests with 5.7 to 7.5 kg of the size fraction 25-40 mm were conducted. More than four tests would have been desirable, but could not be carried out due to a lack of material. The bulk sample was analyzed before and after the test with the vibrating sorter [77] (see Section 2).

The test was simulated with the DEM software ThreeParticle using the novel breakage model. A time step of 5×10^{-6} s and the parameters listed in Table 1 and Table 2 were used. In Figure 9 the collision of the material with the steel plate at the bottom during the shatter test is depicted at different points in time. The color scale represents the particle or fragment mass (blue=0 g, red=48 g). The particle breakage is clearly visible in the simulation.

Due to the probabilistic approach, accurate simulation results in terms of fragment size distribution require a high amount of particles. An investigation in [69] reveals that a minimum of 3000 particles is required for accurate simulation results in this case. This depends on the breakage probabilities. If the particle amount is below, as for the shatter test (160 particles), the impact has to be simulated several times and the average values for the PSD are used.

The comparison of test and simulation results from shatter tests is shown in Figure 10. The fragment size distribution after the drop is displayed (100% 25-40 mm before the drop). Minimal mass losses are considered as fines (<6.3 mm) due to dust generation and losses during fragment collection. The arithmetic average from the four tests and 25 simulations with standard deviations are depicted. The comparison shows satisfying agreement between test and simulation results.

Material	Density [kg/m³]	Poisson's ratio [-]	Shear modulus [MPa]
Sinter (40 mm)	1455	0.25	10
Steel	7850	0.25	210000

Table 1: Material parameters for shatter test simulations

Interaction	Restitution [-]	Static friction [-]	Rolling friction [-]
Sinter-Sinter	0.75	0.62	0.5
Sinter-Steel	0.43	0.839	0.5

Table 2: Interaction parameters for shatter test simulations [86, 87]

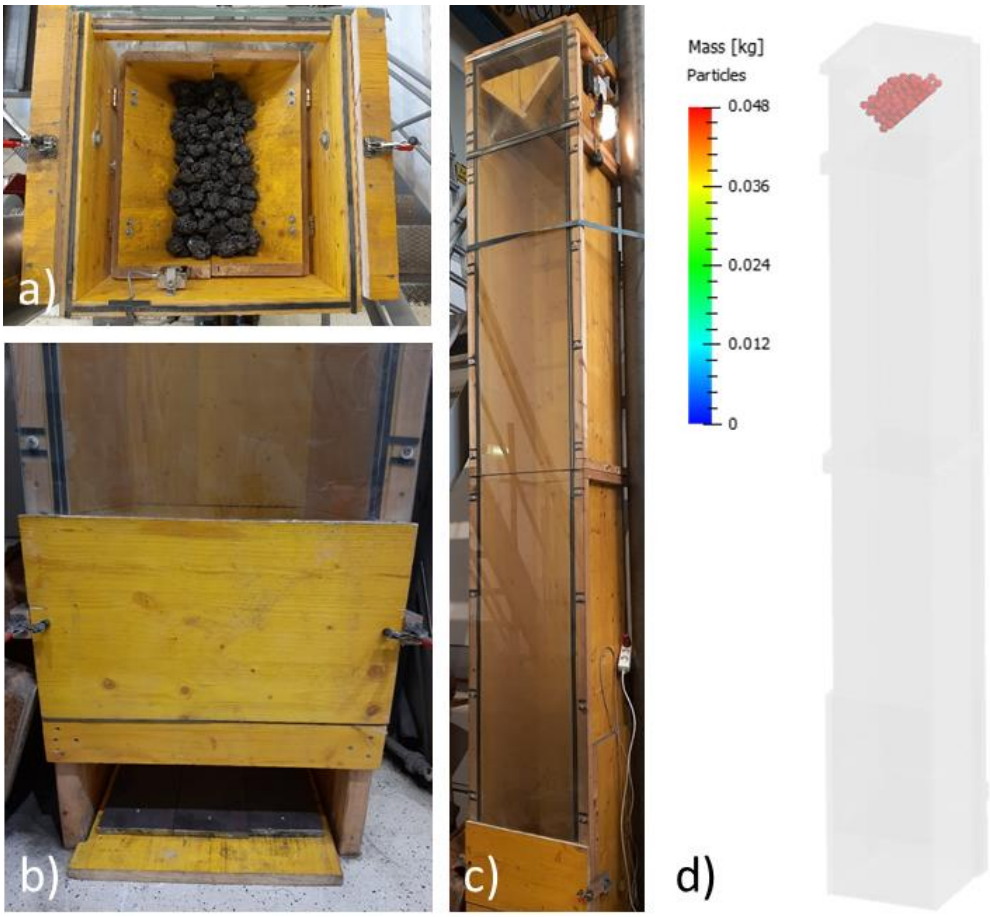

Figure 8: Drop apparatus a) bulk material in quick-opening flap b) steel plate at bottom c) front view d) DE-simulation with ThreeParticle [69]

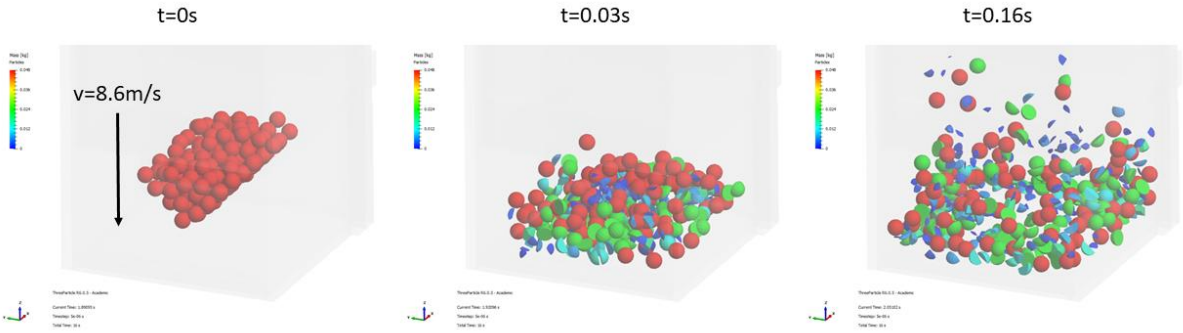

Figure 9: DE-simulation of the shatter test using the novel breakage model showing the collision of the material with the steel plate at different points in time. Color scale represents mass (0-48 g). [69]

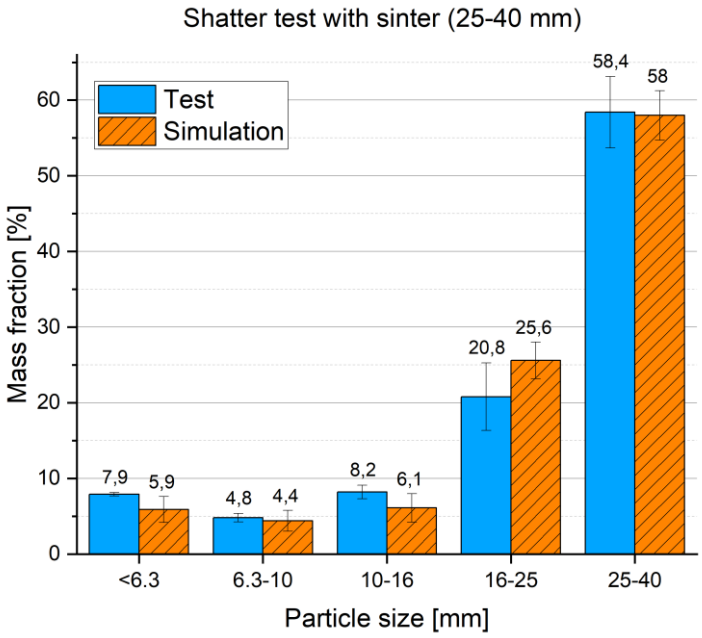

Figure 10: Comparison of test and simulation results from shatter tests [69]

For further validation, bulk material degradation during conveying with two different transfer chutes at the same point was investigated. Originally, this trial was conducted to compare an innovative dynamic transfer system named FlowScrape with a standard chute with regard to particle breakage [5, 6, 88]. The dynamic transfer system FlowScrape consists of 3 rubber tracks, which are linked with cardanic joints for synchronisation and is driven by a friction wheel on the lower belt conveyor. The FlowScrape is patented [89] and described in detail in [90]. A significant reduction of bulk material degradation and in this case 50% less fines generation with the FlowScrape was noticed.

The standard chute is a simple cuboid construction with a baffle plate at the rear wall. The drop height for both systems was 1.6 m and belt conveyor speeds were 1.5 m/s. Sinter with 31-50 mm size from a different manufacturer than for the shatter tests was used. With each system 6 tests were conducted and the PSD before and after the transfer point were measured with the vibrating sorter.

The DE-simulations were conducted with ThreeParticle and a time step of 5 x 10^{-6} s and the parameters listed in Table 3 and Table 4 were used (see Figure 11 and Figure 12). In both simulations 465 kg of sinter was used, which is equivalent to 8319 particles. The color scale represents the particle mass. To represent the size fraction 31.5-50 mm, a particle mix (25, 40 and 50 mm) with the PSD in Table 5, measured in [88], was used. Replacement probabilities in Figure 13 are based on breakage test in [5, 6], where the size fraction 31.5-50 mm with a similar PSD was tested. A detailed description for obtaining the replacement probabilities for a particle mix are provided in [70].

As there are several damaging events, multiple breakage was implemented for this case. All particles and fragments larger than 16 mm were breakable. For particles smaller than 16 mm no breakage was determined in breakage tests at energy levels occurring in these cases [77].

The comparison of test and simulation results is depicted in Figure 14 and Figure 15. The average of each 6 tests is calculated. The increase of mass fractions for each particle size including the standard deviations is depicted. A good agreement of test and simulation results is noticed, especially for fines generation (<6.3mm).

Material	Density [kg/m³]	Poisson's ratio [-]	Shear modulus [MPa]
Sinter (31.5-50 mm)	1908	0.25	10
Steel	7850	0.25	21000
FlowScrape	1400	0.5	7600
Conveyor belt	1400	0.5	7600

Table 3: Material parameters for conveying simulations

Interaction	Restitution [-]	Static friction [-]	Rolling friction [-]
Sinter-Sinter	0.75	0.62	0.5
Sinter-Steel	0.43	0.839	0.5
Sinter-FlowScrape	0.49	0.7	0.5
Sinter-Conveyor belt	0.4	0.7	0.5

Table 4: Interaction parameters for conveying simulations [86, 87]

Size fraction [mm]	Mass fraction (FlowScrape) [%]	Mass fraction (chute) [%]
16-25	15.2	18.2
25-40	74.9	70.3
40-50	9.9	11.5

Table 5: PSD for sinter mix 31.5-50 mm

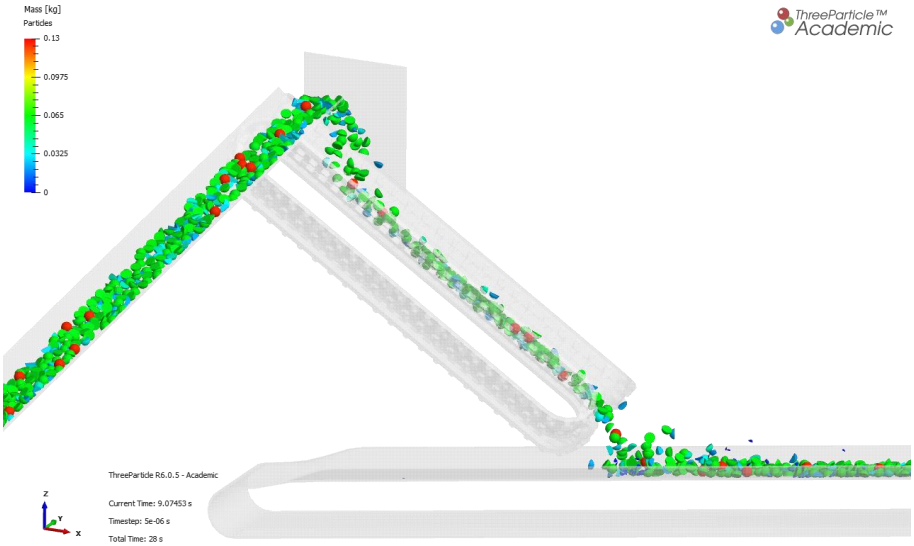

Figure 11: Simulation of the FlowScrape using the novel breakage model with multiple breakage. Color scale represents mass (0 - 0.13 kg) [69]

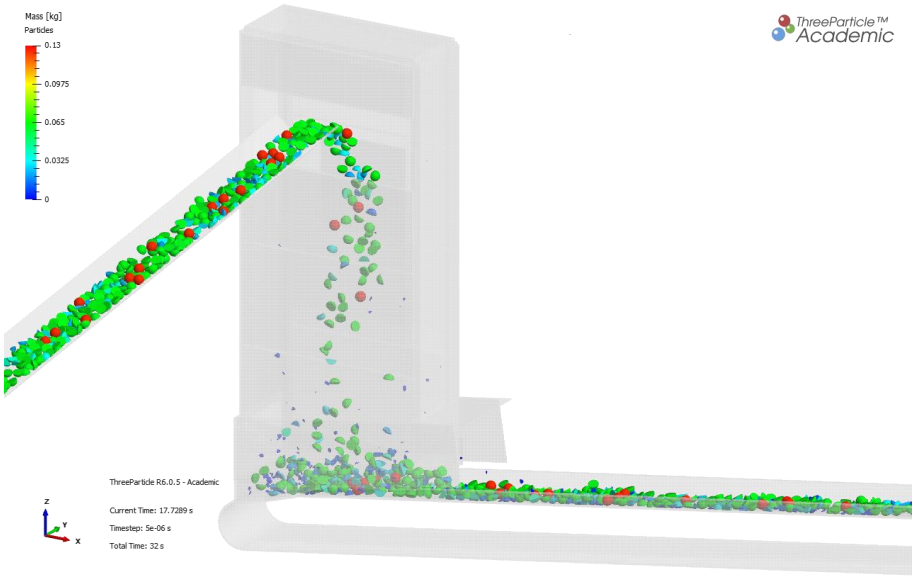

Figure 12: Simulation of the conventional chute using the novel breakage model with multiple breakage. Color scale represents mass (0 - 0.13 kg) [69]

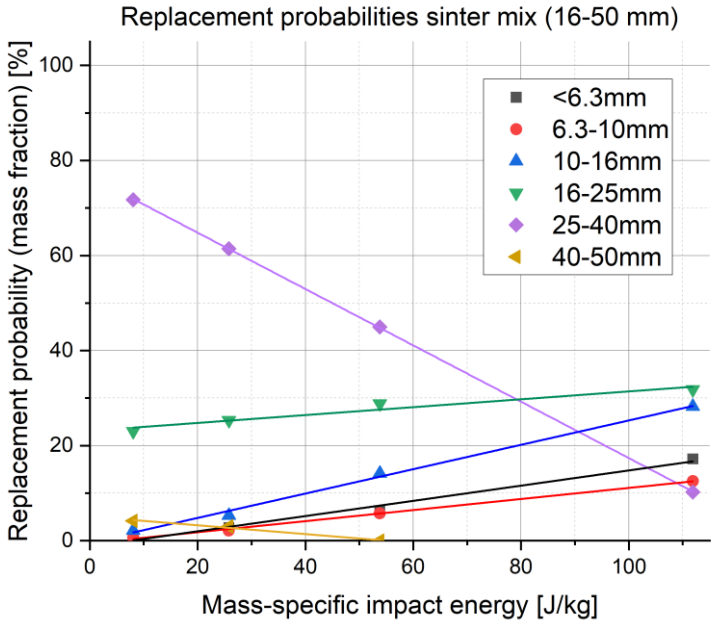

Figure 13: Replacement probabilities for following particles from linear regression for a mix similar to the PSDs in Table 5

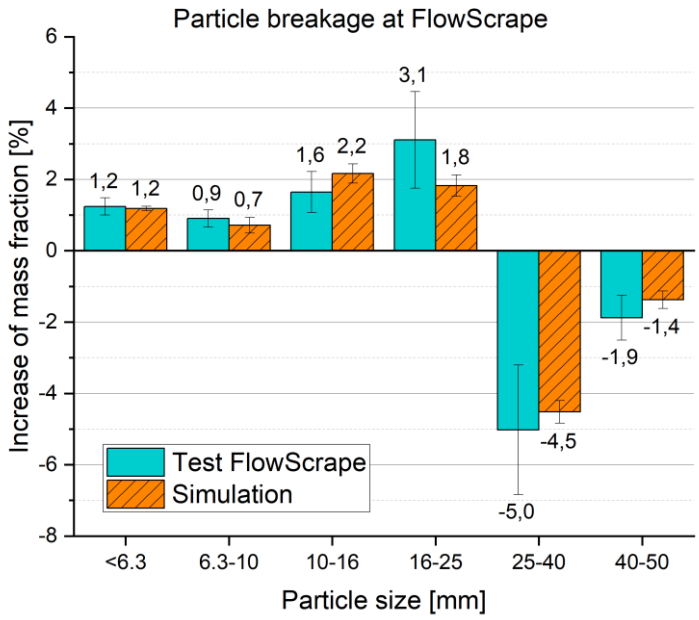

Figure 14: Comparison of test and simulation results: increase of mass fractions due to transfer with the dynamic transfer chute FlowScrape [69]

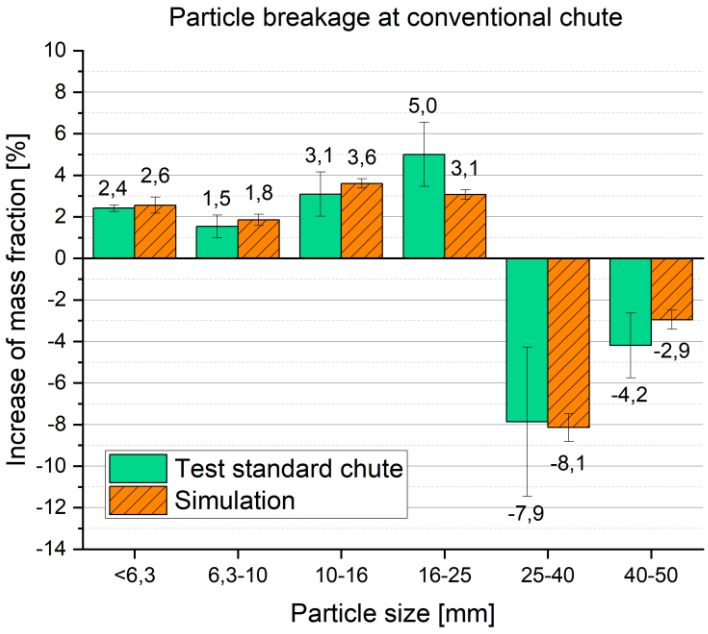

Figure 15: Comparison of test and simulation results: increase of mass fractions due to transfer with the dynamic transfer chute FlowScrape [69]

7. Summary and conclusion

In order to simulate particle breakage in high mass flows with high accuracy in terms of fragment size distribution and reasonable computing efficiency, a novel breakage model was developed for DEM. The model was developed in ThreeParticle's particle replacement API using C++. The model is based on a probabilistic particle replacement with fragments which were previously tessellated with the Voronoi algorithm. Depending on the stress, the particle is replaced by different breakage patterns. The fragments are sharp-edged and of random shape. Slightly more computing power is necessary than for a replacement with spheres, as in [20] for example. The major advantage is, however, that mass and volume constancy is ensured in this model. Initial particles are polyhedral and can be of any shape.

Replacement probabilities for breakage patterns are obtained from breakage tests. By temporarily logging the damage history of particles, compressive force peaks are detected. After every compressive force peak, a random procedure is conducted to determine if a particle breaks and which breakage pattern is applied. This leads to the correct PSD in the bulk sample if applied to a high amount of particles. It has to be stated that energy balance is not correct in the simulations performed in this work because breakage energy was not taken into account due to missing data. This could be corrected by reducing rebound velocity, when breakage energy was known. For this purpose, further investigations regarding breakage energy are necessary.

The correlation of compressive force and impact velocity can be obtained from impact simulations with a high number of particles. The Hooke contact model is more suitable for sharp-edged particles than the Hertz-Mindlin model. More widely dispersed contact forces are noticed with the Hooke model, but no extraordinarily high forces occur as with the Hertz-Mindlin model, which could lead to explosions. Impact simulations revealed that the compressive force due to an impact is only dependent on the particle mass and that it was independent of the particle shape for the Hooke model.

Multiple breakage or further breakage of fragments can also be implemented with this breakage model. This allows to simulate long and complex conveying processes with several damaging events. An example of multiple breakage on three levels is described. The computational scheme of the model is also described in detail.

The novel breakage model was verified and validated with a trial of shatter tests. The results show satisfying agreement of test and simulation

results. Further validations were conducted with a different batch of sinter from a different manufacturer in a trial of conveying tests with a conventional chute and a dynamic transfer system (FlowScrape) including multiple breakage. Also in these cases, satisfying agreement of test and simulation results were noticed, especially in terms of fines generation.

8. Application and Outlook

The breakage model was successfully applied for a solid state material driven turbine used to reduce segregation effects during storage processes [91, 92] or energy recovery [93, 94], which is patented in [95]. Particle breakage due to the turbine was able to be quantified in [70, 92] using the novel breakage model with multiple breakage for a sinter mass flow of 300 t/h. The breakage model is also used to simulate the degradation of Hot Briquetted Iron (HBI) and Direct Reduced Iron (DRI) in two current projects at the Chair of Mining Engineering and Mineral Economics at the University of Leoben.

9. Acknowledgements

This work was conducted within the project MinSiDeg, which received funding from the European Union's Research Fund for Coal and Steel (RFCS) under grant agreement number 847285. Special thanks go to A. Becker from Becker3D for the great software support regarding the simulation software ThreeParticle.

10. References

1. Cundall PA, Strack ODL (1979) A discrete numerical model for granular assemblies. Géotechnique 29:47–65. https://doi.org/10.1680/geot.1979.29.1.47
2. Weerasekara NS, Powell MS, Cleary PW et al. (2013) The contribution of DEM to the science of comminution. Powder Technology 248:3–24. https://doi.org/10.1016/j.powtec.2013.05.032
3. Zhu HP, Zhou ZY, Yang RY et al. (2008) Discrete particle simulation of particulate systems: A review of major applications and findings. Chemical Engineering Science 63:5728–5770. https://doi.org/10.1016/j.ces.2008.08.006
4. Yeom SB, Ha E-S, Kim M-S et al. (2019) Application of the Discrete Element Method for Manufacturing Process Simulation in the Pharmaceutical Industry. Pharmaceutics 11. https://doi.org/10.3390/pharmaceutics11080414
5. Denzel M, Prenner M (2022) Partikelbruchvorhersage an einem dynamischen Übergabesystem und Vergleich mit einer herkömmlichen Schurre mittels DEM (Particle breakage prediction on a dynamic transfer system and comparison with a conventional chute using DEM). Berg Huettenmaenn Monatsh 167:66–75. https://doi.org/10.1007/s00501-022-01197-4

6. Denzel M, Prenner M (2021) Dynamisches Übergabesystem zur Reduktion des Partikelbruchs (Dynamic transfer system to reduce particle breakage). 25. Fachtagung Schüttgutfördertechnik 2021:233–242. https://doi.org/10.25673/36794
7. Powell MS, McBride AT (2006) What is required from DEM simulations to model breakage in mills? Minerals Engineering 19:1013–1021. https://doi.org/10.1016/j.mineng.2006.03.009
8. Tavares LM (2017) A Review of Advanced Ball Mill Modelling. KONA 34:106–124. https://doi.org/10.14356/kona.2017015
9. Beinert S, Fragnière G, Schilde C et al. (2018) Multiscale simulation of fine grinding and dispersing processes: Stressing probability, stressing energy and resultant breakage rate. Advanced Powder Technology 29:573–583. https://doi.org/10.1016/j.apt.2017.11.034
10. Oliveira A, Rodriguez VA, Carvalho RM de et al. (2020) Mechanistic modeling and simulation of a batch vertical stirred mill. Minerals Engineering 156:106487. https://doi.org/10.1016/j.mineng.2020.106487
11. Li H, McDowell G, Lowndes I (2014) Discrete element modelling of a rock cone crusher. Powder Technology 263:151–158. https://doi.org/10.1016/j.powtec.2014.05.004
12. Cleary PW, Sinnott MD (2015) Simulation of particle flows and breakage in crushers using DEM: Part 1 – Compression crushers. Minerals Engineering 74:178–197. https://doi.org/10.1016/j.mineng.2014.10.021
13. Barrios GK, Tavares LM (2016) A preliminary model of high pressure roll grinding using the discrete element method and multi-body dynamics coupling. International Journal of Mineral Processing 156:32–42. https://doi.org/10.1016/j.minpro.2016.06.009
14. André FP, Tavares LM (2020) Simulating a laboratory-scale cone crusher in DEM using polyhedral particles. Powder Technology 372:362–371. https://doi.org/10.1016/j.powtec.2020.06.016
15. Nistala SH, Sinha M, Kumar Choudhary M et al. (2015) Study of generation of sinter return fines during transportation. Ironmaking & Steelmaking 42:226–232. https://doi.org/10.1179/1743281214Y.0000000224
16. Basu S, Chakrabarty A, Nag S et al. (2023) Modeling and simulation of mechanical degradation of iron ore sinter in a complex transfer chute system using the discrete element model and a particle breakage model. Powder Technology:118264. https://doi.org/10.1016/j.powtec.2023.118264
17. Denzel M, Prenner M (2021) Minimierung des Sinterzerfalls mittels DEM (Minimization of Sinter Degradation with DEM). Berg- und Huettenmaennische Monatshefte (BHM) 166:76–81. https://doi.org/10.1007/s00501-021-01081-7
18. Remus R, Aguado-Monsonet MA, Roudier S et al. (2013) Best available techniques (BAT) reference document for iron and steel production: Industrial emissions Directive 2010/75/EU : integrated pollution prevention and control. Scientific and technical research series, vol 25521. Publications Office of the European Union, Luxembourg
19. Prenner M, Denzel M (2022) Projekt MinSiDeg. Stein & Kies (Mitgliederzeitschrift - Forum mineralische Rohstoffe):11
20. Tavares LM, das Chagas AS (2021) A stochastic particle replacement strategy for simulating breakage in DEM. Powder Technology 377:222–232. https://doi.org/10.1016/j.powtec.2020.08.091
21. Potyondy DO, Cundall PA (2004) A bonded-particle model for rock. International Journal of Rock Mechanics and Mining Sciences 41:1329–1364. https://doi.org/10.1016/j.ijrmms.2004.09.011
22. Tan Y, Yang D, Sheng Y (2009) Discrete element method (DEM) modeling of fracture and damage in the machining process of polycrystalline SiC. Journal of the European Ceramic Society 29:1029–1037. https://doi.org/10.1016/j.jeurceramsoc.2008.07.060

23. Kafui K, Thornton C (2000) Numerical simulations of impact breakage of a spherical crystalline agglomerate. Powder Technology 109:113–132. https://doi.org/10.1016/S0032-5910(99)00231-4
24. Metzger MJ, Glasser BJ (2012) Numerical investigation of the breakage of bonded agglomerates during impact. Powder Technology 217:304–314. https://doi.org/10.1016/j.powtec.2011.10.042
25. Khanal M, Schubert W, Tomas J (2008) Oblique Impact Simulations of High Strength Agglomerates. Micro-Macro-Interactions:243–253. https://doi.org/10.1007/978-3-540-85715-0_19
26. Khanal M, Tomas J (2009) Oblique impact simulations of high strength agglomerates. Advanced Powder Technology 20:150–157. https://doi.org/10.1016/j.apt.2008.06.001
27. Antonyuk S, Khanal M, Tomas J et al. (2006) Impact breakage of spherical granules: Experimental study and DEM simulation. Chemical Engineering and Processing: Process Intensification 45:838–856. https://doi.org/10.1016/j.cep.2005.12.005
28. Platzer F, Fimbinger E (2022) Simulation of complex-shaped particle breakage using the Discrete Element Method. Conference: 16. International Conference on Discrete Multiphysics, Modelling Complex Systems with Particle Methods and Discrete Element Method At: Stockholm, Sweden, ISNN: 1307-6892
29. Metzger MJ, Glasser BJ (2013) Simulation of the breakage of bonded agglomerates in a ball mill. Powder Technology 237:286–302. https://doi.org/10.1016/j.powtec.2012.12.006
30. Patwa A, Ambrose RK, Casada M (2016) Discrete element method as an approach to model the wheat milling process. Powder Technology 302:350–356. https://doi.org/10.1016/j.powtec.2016.08.052
31. Quist J, Evertsson CM (2016) Cone crusher modelling and simulation using DEM. Minerals Engineering 85:92–105. https://doi.org/10.1016/j.mineng.2015.11.004
32. Fimbinger E (2021) A Methodology for Dynamic Belt Simulation, Montanuniversität Leoben - University of Leoben. https://doi.org/10.34901/mul.pub.2021.3
33. Orozco LF, Delenne J-Y, Sornay P et al. (2019) Discrete-element model for dynamic fracture of a single particle. International Journal of Solids and Structures 166:47–56. https://doi.org/10.1016/j.ijsolstr.2019.01.033
34. Potapov AV, CAMPBELL CS (1994) Computer simulation of impact-induced particle breakage. Powder Technology 81:207–216. https://doi.org/10.1016/0032-5910(94)02907-5
35. Aström JA, Herrmann HJ (1998) Fragmentation of grains in a two-dimensional packing. The European Physical Journal B:551–554
36. Cleary P (2001) Modelling comminution devices using DEM. Int J Numer Anal Meth Geomech 25:83–105. https://doi.org/10.1002/1096-9853(200101)25:1<83:AID-NAG120>3.0.CO;2-K
37. Cleary PW (2001) Recent advances in dem modelling of tumbling mills. Minerals Engineering 14:1295–1319. https://doi.org/10.1016/S0892-6875(01)00145-5
38. Barrios GK, Jiménez-Herrera N, Tavares LM (2020) Simulation of particle bed breakage by slow compression and impact using a DEM particle replacement model. Advanced Powder Technology 31:2749–2758. https://doi.org/10.1016/j.apt.2020.05.011
39. Brzeziński K, Gladky A (2022) Clump breakage algorithm for DEM simulation of crushable aggregates. Tribology International 173:107661. https://doi.org/10.1016/j.triboint.2022.107661
40. Tavares LM, Rodriguez VA, Sousani M et al. (2021) An effective sphere-based model for breakage simulation in DEM. Powder Technology 392:473–488. https://doi.org/10.1016/j.powtec.2021.07.031
41. Delaney GW, Morrison RD, Sinnott MD et al. (2015) DEM modelling of non-spherical particle breakage and flow in an industrial scale cone crusher. Minerals Engineering 74:112–122. https://doi.org/10.1016/j.mineng.2015.01.013

42. Tavares LM, André FP, Potapov A et al. (2020) Adapting a breakage model to discrete elements using polyhedral particles. Powder Technology 362:208–220. https://doi.org/10.1016/j.powtec.2019.12.007
43. Lichter J, Lim K, Potapov A et al. (2009) New developments in cone crusher performance optimization. Minerals Engineering 22:613–617. https://doi.org/10.1016/j.mineng.2009.04.003
44. Potapov A, Herbst JA, Song M et al. (2007) A DEM-PBM fast breakage model for simulation of comminution processes. Proc. Computational Modeling
45. Arruda Tino AA de, Tavares LM (2022) Simulating breakage tests using the discrete element method with polyhedral particles. Comp Part Mech 9:811–823. https://doi.org/10.1007/s40571-021-00448-4
46. Barrios GK, Pérez-Prim J, Tavares LM (2015) DEM simulation of bed particle compression using the particle replacement model. Proceedings 14th European Symposium on Comminution and Classification
47. Zhou W, Di Wang, Ma G et al. (2020) Discrete element modeling of particle breakage considering different fragment replacement modes. Powder Technology 360:312–323. https://doi.org/10.1016/j.powtec.2019.10.002
48. Cil MB, Buscarnera G (2016) DEM assessment of scaling laws capturing the grain size dependence of yielding in granular soils. Granular Matter 18. https://doi.org/10.1007/s10035-016-0638-9
49. Rodriguez VA, Barrios GKP, Bueno G et al. (2021) Investigation of Lateral Confinement, Roller Aspect Ratio and Wear Condition on HPGR Performance Using DEM-MBD-PRM Simulations. Minerals 11:801. https://doi.org/10.3390/min11080801
50. Sousani M, Chagas A, Saxena A et al. (2019) Simulation of Surface Damage and Body Breakage by using DEM
51. Tavares LM (2022) Review and Further Validation of a Practical Single-Particle Breakage Model. KONA 39:62–83. https://doi.org/10.14356/kona.2022012
52. Tavares L, King R (1998) Single-particle fracture under impact loading. International Journal of Mineral Processing 54:1–28. https://doi.org/10.1016/S0301-7516(98)00005-2
53. Rocky DEM Inc. (2018) Tavares Breakage Model in Rocky DEM. https://rocky.esss.co/blog/tavares-breakage-model-in-rocky-dem/. Accessed 09 Sep 2022
54. Potapov A, Donohue T, Ilic D Computer Simulation of Coal Breakage in Conveyor Transfer Chutes with ROCKY Discrete Element Method Package. Rocky DEM Technical Articles
55. Voronoi G (1908) Nouvelles applications des paramètres continus à la théorie des formes quadratiques. Deuxième mémoire. Recherches sur les parallélloèdres primitifs. Journal für die reine und angewandte Mathematik (Crelles Journal) 1908:198–287. https://doi.org/10.1515/crll.1908.134.198
56. Voronoi G (1908) Nouvelles applications des paramètres continus à la théorie des formes quadratiques. Premier mémoire. Sur quelques propriétés des formes quadratiques positives parfaites. Journal für die reine und angewandte Mathematik (Crelles Journal) 1908:97–102. https://doi.org/10.1515/crll.1908.133.97
57. Wejrzanowski T, Skibinski J, Szumbarski J et al. (2013) Structure of foams modeled by Laguerre–Voronoi tessellations. Computational Materials Science 67:216–221. https://doi.org/10.1016/j.commatsci.2012.08.046
58. Duan Q, Kroese DP, Brereton T et al. (2014) Inverting Laguerre Tessellations. The Computer Journal 57:1431–1440. https://doi.org/10.1093/comjnl/bxu029
59. Flavio A, Potapov A, Tavares LM (2019) Simulation of single particle breakage using non-round particles in ROCKY DEM. 26th International Mining Congress and Mining Exhibition of Turkey
60. Potapov A, CAMPBELL CS (1996) A three-dimensional simulation of brittle solid fracture. Int J Mod Phys C 07:717–729. https://doi.org/10.1142/S0129183196000594

61. Potapov AV, CAMPBELL CS (2000) The breakage induced by a single grinding ball dropped onto a randomly packed particle bed. Powder Technology 107:108–117. https://doi.org/10.1016/S0032-5910(99)00177-1
62. Paluszny A, Tang X, Nejati M et al. (2016) A direct fragmentation method with Weibull function distribution of sizes based on finite- and discrete element simulations. International Journal of Solids and Structures 80:38–51. https://doi.org/10.1016/j.ijsolstr.2015.10.019
63. Herbst JA, Potapov AV (2004) Making a Discrete Grain Breakage model practical for comminution equipment performance simulation. Powder Technology 143-144:144–150. https://doi.org/10.1016/j.powtec.2004.04.036
64. Jiménez-Herrera N, Barrios GK, Tavares LM (2017) Comparison of breakage models in DEM in simulating impact on particle beds. Advanced Powder Technology 29:692–706. https://doi.org/10.1016/j.apt.2017.12.006
65. Potapov AV, CAMPBELL CS (1997) The two mechanisms of particle impact breakage and the velocity effect. Powder Technology 93:13–21. https://doi.org/10.1016/S0032-5910(97)03242-7
66. Petit HA, Potapov A, Tavares LM (2022) Simulation of breakage of iron ore pellets using the discrete breakage model. 17th European Symposium on Comminution & Classification (ESCC 2022)
67. Denzel M (2022) Partikelbruch in der Fördertechnik - Prüfmethodik und Simulation mittels Diskrete Elemente Methode (Particle breakage during conveying processes - Test method and simulation with the discrete element method). In: Langefeld O (ed) 10. Kolloquium - Fördertechnik im Bergbau, 1st edn. Papierflieger Verlag GmbH, Clausthal-Zellerfeld, pp 89–101
68. Denzel M (2022) Partikelbruch in der Fördertechnik: Prüfmethodik und Simulation mittels Diskrete Elemente Methode. Bergbau - Zeitschrift für Rohstoffgewinnung, Energie, Umwelt 73:436–440. https://doi.org/10.34901/mul.pub.2023.03
69. Denzel M, Prenner M, Sifferlinger NA (2022) A probabilistic particle replacement model to simulate bulk material degradation during conveying processes using DEM. Montanuniversität Leoben. Proceedings MHCL 2022 - 24th International Conference on Material Handling, Constructions and Logistics in Belgrad, Serbia:29–36. https://doi.org/10.34901/mul.pub.2023.02
70. Denzel M (2023) A Breakage Model for Discrete Element Simulations Applied to Iron Ore Sinter. PhD Thesis, University of Leoben. https://doi.org/10.34901/mul.pub.2023.01
71. Faramarzi F, Napier-Munn T, Morrison R et al. (2020) The extended drop weight testing approach – What it reveals. Minerals Engineering 157:106550. https://doi.org/10.1016/j.mineng.2020.106550
72. Faramarzi F, Jokovic V, Morrison R et al. (2018) Quantifying variability of ore breakage by impact – Implications for SAG mill performance. Minerals Engineering 127:81–89. https://doi.org/10.1016/j.mineng.2018.07.007
73. Kotzur BA, Berry RJ, Zigan S et al. (2018) Particle attrition mechanisms, their characterisation, and application to horizontal lean phase pneumatic conveying systems: A review. Powder Technology 334:76–105. https://doi.org/10.1016/j.powtec.2018.04.047
74. Cavalcanti PP, Petit HA, Thomazini AD et al. (2021) Modeling of degradation by impact of individual iron ore pellets. Powder Technology 378:795–807. https://doi.org/10.1016/j.powtec.2020.10.037
75. Shi F, Kojovic T, Larbi-Bram S et al. (2009) Development of a rapid particle breakage characterisation device – The JKRBT. Minerals Engineering 22:602–612. https://doi.org/10.1016/j.mineng.2009.05.001
76. Zuo W, Shi F (2016) Ore impact breakage characterisation using mixed particles in wide size range. Minerals Engineering 86:96–103. https://doi.org/10.1016/j.mineng.2015.12.007

77. Denzel M, Prenner M, Sifferlinger NA (2022) Development of an automated single particle impact tester for iron ore sinter. Minerals Engineering 175:107291. https://doi.org/10.1016/j.mineng.2021.107291
78. Shi F, Kojovic T (2007) Validation of a model for impact breakage incorporating particle size effect. International Journal of Mineral Processing 82:156–163. https://doi.org/10.1016/j.minpro.2006.09.006
79. Albertin G (2013) Piecewise linear least square fit
80. Zhao S, Evans TM, Zhou X (2018) Effects of curvature-related DEM contact model on the macro- and micro-mechanical behaviours of granular soils. Géotechnique 68:1085–1098. https://doi.org/10.1680/jgeot.17.P.158
81. Griffith AA (1921) VI. The phenomena of rupture and flow in solids. Phil Trans R Soc Lond A 221:163–198. https://doi.org/10.1098/rsta.1921.0006
82. Zehnder AT (2013) Griffith Theory of Fracture:1570–1573. https://doi.org/10.1007/978-0-387-92897-5_259
83. Becker A (2022) Discrete Element Method (Becker3D)
84. Matsumoto M, Nishimura T (1998) Mersenne twister. A 623-dimensionally equidistributed uniform pseudorandom number generator. ACM Transactions on Modeling and Computer Simulation:3–30
85. Grübler C (2020) Evaluierung ausgewählter passiver staubreduktionsmaßnahmen beim Schüttgutumschlag an fördertechnischen Anlagen (Evaluation of passive dust reducing measures at bulk material handling on conveying equipment). PhD Thesis, University of Leoben
86. Prenner M (2018) Simulationsparameterstudie - Sinterbunker (Simulation parameter study - Sinter bunkers). Project report, University of Leoben
87. Brugger M (2021) Rücksprungverhalten von Hochofensinter (Rebound behaviour of blast furnace sinter). Bachelor Thesis, University of Leoben
88. Wagner P (2022) Vergleich zweier Übergabeeinrichtungen in Bezug auf Partikelbruch (Comparison of two transfer systems with regard to particle breakage). Master's Thesis, University of Leoben
89. Dünnwald W, Prenner M (2019) Vorrichtung zum Leiten eines von einem Abwurfende oder Austragsende einer Fördereinrichtung abfließenden Materialstroms (Device for guiding a material flow flowing out from a discharge end or delivery end of a conveying apparatus). Patentnr. DE 10 2019 108 687 A1. Deutschland
90. Prenner M (2021) Dynamische Übergabeschurre zur Effizienzsteigerung von Gurtbandförderern (Dynamic Transfer Chute to Improve Efficiency of Belt Conveyors). Berg Huttenmannische Monatshefte:1–6. https://doi.org/10.1007/s00501-021-01084-4
91. Denzel M, Prenner M (2022) Solid State Material Driven Turbine to Reduce Segregation Effects in Bunkers. In: CHoPS 2022 - 10th International Conference on Conveying and Handling of Particulate Solids, Salerno, Italy
92. Denzel M, Prenner M, Sifferlinger NA (2023) Solid State Material Driven Turbine to Reduce Segregation during Bunker Filling. Berg Huettenmaenn Monatsh. https://doi.org/10.1007/s00501-022-01311-6
93. Prenner M (2015) Feststoffturbine zur Energierückgewinnung in Kombination mit Gurtförderanlagen. Berg Huettenmaenn Monatsh 160:21–31. https://doi.org/10.1007/s00501-014-0327-0
94. Prenner M, Grübler C, Zeiler S (2018) Vorteile von Feststoffturbinen. Schüttgut:68–72
95. Prenner M (2012) Solid state material driven turbine: International Patent F03G3/02 F03G3/04(WO 2013/083303 A1)